NUCL SCI TECH (2022) 33:111
https://doi.org/10.1007/s41365-022-01096-w

Configurational information entropy analysis of fragment mass cross distributions to determine the neutron skin thickness of projectile nuclei

Hui-Ling Wei[1] · Xun Zhu[1] · Chen Yuan[1]

Received: 29 July 2022 / Revised: 20 August 2022 / Accepted: 27 August 2022 / Published online: 13 September 2022

Abstract Configurational information entropy (CIE) analysis has been shown to be applicable for determining the neutron skin thickness ($\delta_{\rm np}$) of neutron-rich nuclei from fragment production in projectile fragmentation reactions. The BNN + FRACS machine learning model was adopted to predict the fragment mass cross-sections (σ_A) of the projectile fragmentation reactions induced by calcium isotopes from ^{36}Ca to ^{56}Ca on a ^{9}Be target at 140 MeV/u. The fast Fourier transform was adopted to decompose the possible information compositions in σ_A distributions and determine the quantity of CIE ($S_A[f]$). It was found that the range of fragments significantly influences the quantity of $S_A[f]$, which results in different trends of $S_A[f] \sim \delta_{\rm np}$ correlation. The linear $S_A[f] \sim \delta_{\rm np}$ correlation in a previous study [Nucl. Sci. Tech. 33, 6 (2022)] could be reproduced using fragments with relatively large mass fragments, which verifies that $S_A[f]$ determined from fragment σ_A is sensitive to the neutron skin thickness of neutron-rich isotopes.

Keywords Neutron skin thickness · Mass cross-section distribution · Configurational information entropy · Projectile fragmentation reaction

This work was supported by the National Natural Science Foundation of China (No. 11975091) and the Program for Innovative Research Team (in Science and Technology) in the University of Henan Province, China (No. 21IRTSTHN011).

✉ Hui-Ling Wei
htuwhling@126.com

1 College of Physics, Henan Normal University, Xinxiang 453007, China

1 Introduction

In the neutron-rich nucleeus, valence neutrons may have a large spatial extension, causing them to form a thick skin structure or even an exotic giant neutron halo for near-dripline nuclei [1–3]. Defined as the difference between the point neutron and proton root-mean-square radii ($\delta_{\rm np} = \delta_{\rm n} - \delta_{\rm p}$) of a nucleus, the neutron skin thickness reflects the difference between the nuclear density distributions of neutrons and protons. The neutron skin thickness is an important parameter for constraining the nuclear symmetry energy and nuclear equation of state. In the newly opened Facility for Rare Ion Beams (FRIB), USA, and other building factories, such as the High-Intensity Heavy Ion Accelerator Facility (HIAF), China, a variety of new isotopes are expected to be created with advanced technologies in beam intensity and particle identification, which makes it possible to employ unstable nuclear beams to study neutron halos or even neutron clusters [4]. Because of difficulties in the direct measurement of neutrons, the neutron skin thickness is always determined using many probes in nuclear reactions, such as the reaction cross-section or interaction cross-section, ratios of charged particles, nucleon removal cross-sections, or others sensitive to the change in neutron density distribution (see recent reviews in [4, 5]).

The projectile fragmentation (PF) reaction is a violent reaction induced by heavy ions at incident energies above a few tens of MeV/u. It is generally believed to have three processes in transport models (or two processes in some simpler models), that is, the collision, expansion, and subsequent secondary decay process, which sees a corresponding change in information entropy along different collision processes and can be reflected by fragment distributions [5]. The isospin effect in fragment production, that is, the neutron-rich fragments, will be enhanced in a more neutron-rich reaction system, making it useful for determining the neutron density distribution in the projectile nucleus [6–8] or nuclear symmetry energy [9, 10]. In a recent study [Nucl. Sci. Tech. 33, 6 (2022)], employing a modified statistical abrasion-ablation (SAA) model to predict fragment production, configurational information entropy (CIE) analysis was adopted to study the neutron skin thickness of neutron-rich nuclei through fragment distributions in PF reactions [11]. It has been illustrated that the quantities of CIE determined from mass distributions or charge distributions linearly decrease with increasing neutron skin thickness of neutron-rich nuclei. Considering that the SAA model cannot adequately reproduce the mass distribution for light fragments, the CIE analysis of the fragment distribution has been limited to fragments with mass number $A_f \geq 10$ or charge number $Z_f \geq 10$. On the other hand, light fragments also have different production mechanisms than large mass fragments, which mainly account for peripheral collisions. In this study, both light and large fragments were analyzed using the CIE method, based on predictions of a newly developed machine learning model, and the fragment size dependence of CIE in PF reactions was studied.

To obtain the fragment mass cross-section (σ_A) distribution in PF reactions, a precise model prediction of fragment production is required. Among the many parameterizations used to predict fragment cross-sections, FRACS has been proven to be of good quality [12], which incorporates the incident energy dependence of the reaction and odd-even staggering (OES) effects in the fragments. Moreover, machine learning models, such as the Bayesian neural network (BNN), have also been suggested for constructing new models to predict fragment production in PF reactions [13] as well as spallation reactions [14–16]. It was found that, under the guidance of physical models, BNN technology can improve the quality of physical models and the simple BNN model [13, 15, 16]. The recently proposed BNN + FRACS model shows a high prediction quality for fragment cross-sections in PF reactions [13] based on the advantages of the BNN and FRACS models, which makes it possible to simulate both small-mass and large-mass fragments well.

In this study, the BNN + FRACS model was adopted to predict the fragment σ_A distributions in calcium isotope-induced PF reactions, and CIE analysis was used to determine the quantity of CIE for fragment distributions. A further study on the correlation between CIE and the neutron skin thickness of calcium isotopes was performed. These models are described in Sect. 2. In Sect. 3, the results and discussion are shown. The conclusions of this study are presented in Sect. 4.

2 Model description

In this section, the adopted models are described briefly. CIE analysis can be divided into two types, considering that the distribution is discrete or continuous. Because fragments produced in PF reactions are discrete particles, only the CIE analysis of the discrete distribution will be introduced in Sect. 2.1. In Sect. 2.2 and 2.3, the main characteristics of the FRACS and BNN + FRACS models will be briefly introduced, respectively.

2.1 Method of determining CIE from a physical distribution

The quantity of CIE determines chaotic information from a distribution, which usually partially reflects that of the system [17]. Fragment production is considered localized as clusters in heavy-ion collisions, and this method focuses on determining the CIE of a system with spatially localized clusters. The first step starts with the Fourier transform (FT) of a set of functions describing the system $f(x) \in L^2(\mathbf{R})$,

$$\int_{-\infty}^{\infty} |f(x)|^2 \mathrm{d}x = \int_{-\infty}^{\infty} |F(k)|^2 \mathrm{d}k, \tag{1}$$

which obeys Plancherel's theorem [18]. $f(x)$ must be a bounded squared-integrable function. Thus, $\{F(k)\}$ denotes the frequency-domain signal sequence of the original signal sequence $\{X_n\}$. From $F(k)$, the fraction $f(k)$ in the k mode can be defined [18] as

$$f(k) = \frac{|F(k)|^2}{\int |F(k)|^2 \mathrm{d}^d k}, \tag{2}$$

and the integration is over all k in which $F(k)$ is defined. $\{f(k)\}$ is the normalized frequency-domain signal sequence, for which $f(k)$ denotes the normalized fraction in the k mode. d denotes the number of spatial dimensions. From this definition, it is known that $f(k)$ measures the relative weight of a given mode k and is always smaller than 1. The CIE is defined based on $f(k)$ according to the form of Shannon information entropy [19],

$$S[f] = -\sum_{m=1}^{k} f(m) \ln f(m). \tag{3}$$

In this manner, the quantity of CIE is composed of the information entropy for configurations compatible with certain constraints on a physical system. When each mode k is even in the CIE, $f(m) = 1/N$, and the discrete configuration entropy has a maximum at $S[f] = \ln N$. Under extreme conditions in which there is only one mode of k, $S[f] = 0$. For a continuous distribution, the continuous CIE can be defined [11]. The flowchart in Fig. 1 shows the method of obtaining CIE from an original signal sequence X_n according to the procedures described in Sec. 2.1.

The fast Fourier transform (FFT) was chosen to analyze the fragment cross-section distribution,

$$F(k) = \frac{1}{N}\sum_{n=0}^{N-1} X_n e^{-i2\pi kn}, \tag{4}$$

where $k = m/N$, $0 \le m \le N-1$, and N is the amount of data in the X_n distribution.

2.2 FRACS model

Considering the numerous physical parameters that influence fragment production in PF reactions, the FRACS model can yield good predictions for fragments in PF reactions above 100 MeV/u [12]. The FRACS model improves upon the well-known EPAX3 [20] model by including the energy dependence of fragment production as well as the OES phenomenon in fragments. For a fragment with specific mass and charge numbers $(A_\mathrm{f}, Z_\mathrm{f})$, its cross-section is predicted by

$$\sigma(A_\mathrm{f}, Z_\mathrm{f}) = Y(A_\mathrm{f})Y(Z_\mathrm{prob} - Z_\mathrm{f})\delta_\mathrm{OES}(A_\mathrm{f}, Z_\mathrm{f}), \tag{5}$$

where $Y(A_\mathrm{f})$ refers to the fragment mass cross-section, $Y(Z_\mathrm{prob} - Z_\mathrm{f})$ describes the isobaric distribution, and $\delta_\mathrm{OES}(A_\mathrm{f}, Z_\mathrm{f})$ denotes OES in fragment production.

In this study, $Y(A_\mathrm{f})$ was focused on to extract CIE. According to FRACS, $Y(A_\mathrm{f})$ is given by the following formula:

$$Y(A_\mathrm{f}) = \sigma_\mathrm{R} P \exp[-P(A_\mathrm{p} - A)], \tag{6}$$

where σ_R is the geometrical scaling factor, and P is the slope of this exponential. The physical quantities of σ_R and P are related to the masses of the projectile and target nuclei, as well as the incident energy of the reaction. The parameters for σ_R and P make FRACS agree well with the experimental data. A detailed description of the FRACS model is provided in [12].

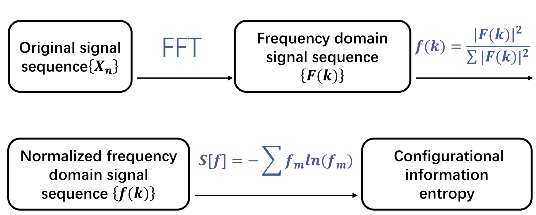

Fig. 1 (Color online) Flow chart of CIE extraction from the original signal sequence $\{X_n\}$ of a physical distribution. The main procedure includes the FFT of the original signal sequence, obtaining the frequency-domain signal sequence $\{F(k)\}$, the normalization to the frequency-domain signal sequence for $\{f(k)\}$, and the calculation of configurational information entropy ($S[f]$) using the Shannon information entropy formula

2.3 BNN + FRACS machine learning model

In a recent study, the BNN + FRACS machine learning model was proposed to predict the fragment cross-section in PF reactions. A detailed description is provided in [13]. In short, the BNN + FRACS model combines the advantages of the FRACS model and the strong learning ability of the BNN to big data, which improves the prediction abilities of both the BNN and FRACS models.

The main characteristics of the BNN + FRACS model are as follows: Under the supervision of the FRACS model, a predictive model was constructed using BNN technology based on massive learning of the difference between the measured fragments and the FRACS prediction in various reactions,

$$\Delta = \lg \sigma_\mathrm{exp} - \lg \sigma_\mathrm{FRACS}, \tag{7}$$

where σ_exp and σ_FRACS denote the measured data and FRACS prediction, respectively.

After a careful comparison of different neural nodes in the hidden layer, the optimized structure of the BNN + FRACS model was found to be formed by one input layer with seven input parameters, one hidden layer with 46 neural units, and one output layer with one output parameter. The input parameters were $(E, A_\mathrm{p}, Z_\mathrm{p}, A_\mathrm{t}, Z_\mathrm{t}, A_\mathrm{f}, Z_\mathrm{f})$, where E is the incident energy in MeV/u, A and Z are the mass and charge numbers, and the sub-indexes p, t, f refer to the projectile, target, and fragment, respectively. A total of 6393 fragments from 53 measured PF reactions were included in the learning dataset, which made it possible for the BNN + FRACS model to reproduce a wide range of fragments with incident energies from 40 to 1 GeV/u and reactions induced by projectile nuclei from ^{40}Ar to ^{208}Pb. The BNN + FRACS model was selected to generate fragment mass cross-sections in PF reactions for its good reproduction of a wide range of fragments. Refer to [13] for a detailed description of the BNN + FRACS model.

3 Results and discussion

The fragment mass cross-sections for 140 MeV/u $^{36-56}$Ca + ^{9}Be reactions were predicted using the BNN + FRACS model. To establish the correlation between CIE and the neutron skin thickness, the double-parameter Fermi-type nuclear density distribution was adopted for neutrons and protons.

$$\rho_i(r) = \frac{\rho_i^0}{1 + \exp(\frac{r - C_i}{t_i/4.4})}, \quad i = \mathrm{n, p} \tag{8}$$

where i denotes neutrons or protons, ρ_i^0 is the normalization constant, t_i is the diffuseness parameter, and C_i is half the density radius of the nuclear density distribution. The neutron skin thickness of the projectile nucleus can be calculated from the ρ_n and ρ_p distributions according to the following definition:

$$\delta_\mathrm{np} = \sqrt{\langle r_\mathrm{n}^2 \rangle} - \sqrt{\langle r_\mathrm{p}^2 \rangle}. \tag{9}$$

The fragment σ_A distributions for a series of 140 MeV/u $^{36-56}$Ca + ^{9}Be reactions are shown in Fig. 2. More results have been predicted, but only some of them were plotted for concise discussion. Because the mass number of fragments reflects the colliding area, the ratio of the fragment mass to that of the projectile nucleus $A_\mathrm{f}/A_\mathrm{P}$ was adopted as a cut for the upper limitation when selecting the fragment range for the FFT analysis. In addition, to better discuss the mass distribution, a cut was made to $A_\mathrm{f} \leq 90\% A_\mathrm{P}$ to avoid imprecise fragment predictions in peripheral collisions by the BNN + FRACS model. After the fragment cuts, the $\{\sigma_A\}$ sequence served as data group $\{X_\mathrm{n}\}$ in Eq. (4), which was performed using the FFT analysis. From the reaction of ^{36}Ca to ^{48}Ca, the σ_A distributions generally exhibited similar trends, which can be divided into two parts: the first for the light mass fragment, where σ_A decreased rapidly within the range $A_\mathrm{f} \leq \sim 14$, and the second, where σ_A increased with A_f within the range $\sim 14 \leq A \leq 90\% A_\mathrm{P}$. There was an additional part in the σ_A distribution of the ^{52}Ca-induced reaction and in the reactions of projectile nuclei larger than ^{52}Ca. Compared to the experimental results for the 140 MeV/u ^{40}Ca + ^{9}Be (open squares) and ^{48}Ca + ^{9}Be (open circles) reactions [21], the BNN + FRACS model effectively reproduced the measured σ_A distributions, which made it possible to carry out a CIE analysis of the mass distribution for reactions induced by calcium isotopes with different isospins.

Taking the 140 MeV/u ^{44}Ca + ^{9}Be reaction as an example, the FFT analysis of the σ_A distribution is shown. In the analysis, the upper limitations on the fragments were set as $60\% A_\mathrm{P}$ to $90\% A_\mathrm{P}$ (in steps of $5\% A_\mathrm{P}$) to observe the influence of fragment size, which indicates the percentage of projectiles involved in the collision and the neutron skin effect. The results are presented in Fig. 3. In general, except for the first peak, the amplitude $F(k)$ decreased as the mode k increased. At approximately $k = 0.23$, a second weak peak was found with upper limitations on the fragments of $A_\mathrm{f} \leq 70\% A_\mathrm{P}$. With an increase in the upper mass limitation, the distribution of the FFT spectrum gradually decreased.

Using Eq. (3), the CIE for fragment σ_A distributions was calculated from the FFT analysis, which is labeled as $S_A[f]$. The results of $S_A[f]$ and their correlation with δ_np for the 140 MeV/u ^{A_P}Ca + ^{9}Be reactions are plotted in Fig. 4, in which A_P ranges from 36 to 56, and the upper limitations on fragments masses are changed from $60\% A_\mathrm{P}$ to $90\% A_\mathrm{P}$. δ_np of the projectile nucleus was calculated using the nuclear density distribution according to Eq. (8). Around ^{43,44}Ca, $\delta_\mathrm{np} \sim 0$, indicating proton skins in $^{36-42}$Ca, and

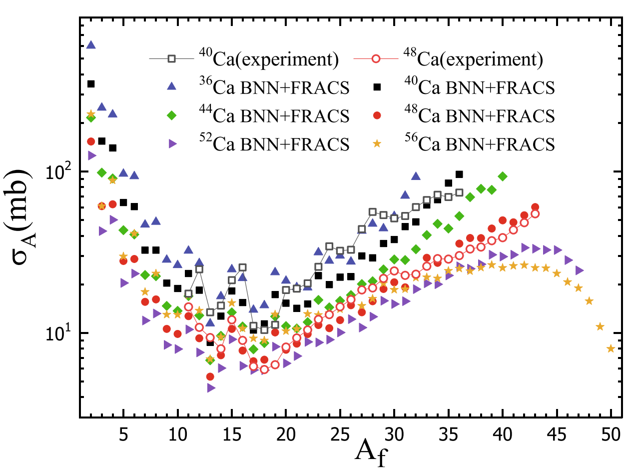

Fig. 2 (Color online) Predicted mass cross-section (σ_A) distributions using the BNN + FRACS model (in solid symbols) for 140 MeV/u ^{A_P}Ca + ^{9}Be reactions. The y-axis denotes σ_A in mb, and the x-axis shows the mass numbers of fragments. The projectile nucleus ranges from the proton-rich ^{36}Ca to the neutron-rich ^{56}Ca, and A_P is changed from 36 to 56 in steps of 4. The measured data in [21] are plotted as open symbols

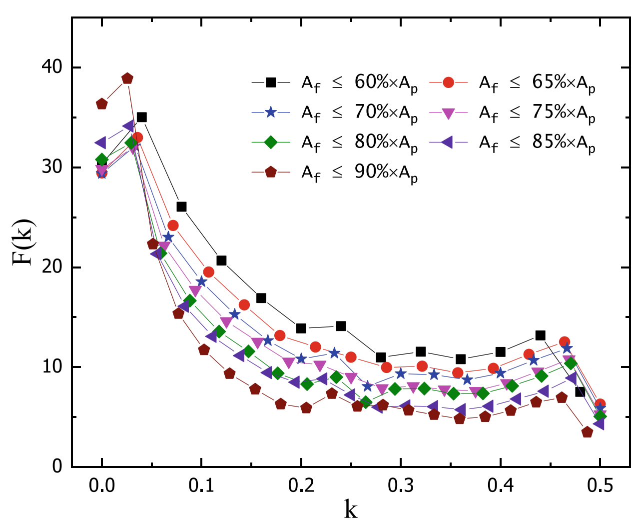

Fig. 3 (Color online) Fast Fourier transform (FFT) of σ_A distributions for the 140 MeV/u ^{44}Ca + ^{9}Be reactions, as plotted in Fig. 2. The x-axis denotes the mode of k, and $F(k)$ is the amplitude of mode k. FFT is performed on fragment cuts from $60\% A_\mathrm{P}$ to $90\% A_\mathrm{P}$ to study the influence of fragment range and fragment size on CIE

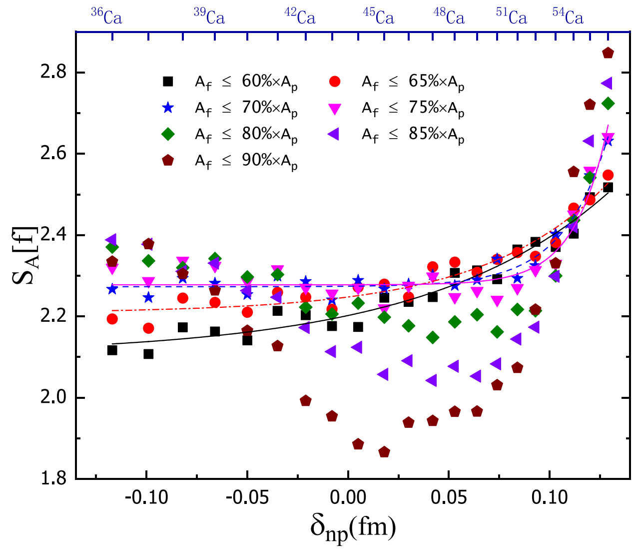

Fig. 4 (Color online) Correlation between $S_A[f]$ obtained from the fragment σ_A distribution and δ_{np} of the projectile nucleus for the 140 MeV/u ^{A_P}Ca + ^{9}Be reactions. A_P ranges from 36 to 56, which covers both the neutron-deficient and neutron-rich calcium isotopes. The bottom x and upper axes denote the neutron skin thickness δ_{np} and corresponding projectile nuclei, respectively. The fragments mass, with upper limitations from 60%A_P to 90%A_P(in steps of 5%A_P), of projectile nuclei are plotted with solid symbols. Except for the 80%A_P, 85%A_P, and 90%A_P upper limitations, the lines denote the exponential fittings to the $S_A[f] \sim \delta_{np}$ correlations, except those of $A_f \leq 85\% A_P$ and $A_f \leq 90\% A_P$

neutron skins in $^{45-60}$Ca. The quantity of $S_A[f]$ determined from the fragment σ_A distribution was not well correlated with δ_{np}. In general, with different upper limitations on fragment mass, $S_A[f]$ was mainly influenced by the relatively neutron-deficient $^{36-43}$Ca reactions, showing an increase with the upper limitation on the fragment mass. It was also observed that $S_A[f]$ gradually increased with δ_{np} for $^{36-42}$Ca, whereas it rapidly increased with δ_{np} for $^{45-56}$Ca. Note that with a fragment upper limitation of 80%A_P, $S_A[f]$ decreased with increasing δ_{np} when $\delta_{np} < 0.03$ fm, whereas the opposite trend occurred when $\delta_{np} > 0.03$ fm. More clearly, with the upper limitations of $A_f \leq 85\% A_P$ and $A_f \leq 90\% A_P$, $S_A[f]$ decreased with δ_{np} when $\delta_{np} < 0.02$ and then increased with δ_{np} in the more neutron-rich nuclei-induced reactions.

Remembering the $S_A[f] \sim \delta_{np}$ correlation predicted by the modified SAA model in [11], $S_A[f]$ was found to linearly decrease with increasing δ_{np} of neutron-rich calcium isotopes from ^{40}Ca to ^{60}Ca. The results do not seem to agree with previous findings. While exploring how this disagreement could have emerged, it was found that the mass distributions adopted in [11] only included fragments with $A_f \geq 10$, whereas in this study, A_f was extended to fragments as light as $A_f = 2$. The inclusion of light fragments may be the reason for this disagreement. Considering this difference, the CIE analysis was re-performed by dividing the fragments into two groups for the case of $A_f \leq 90\% A_P$, that is, $A_f \leq 14$ and $15 \leq A_f \leq 90\% A_P$. The determined $S_A[f]$ and its correlation with δ_{np} of the projectile nuclei are plotted in Fig. 5. Within the range $A_f \leq 14$, $S_A[f]$ decreased very slowly when $\delta_{np} < 0$ and increased with δ_{np} for the more neutron-rich projectiles with thicker neutron skins. An opposite trend is found for the fragments within $15 \leq A_f \leq 90\% A_P$, that is, for $\delta_{np} < 0$, $S_A[f]$ increased with δ_{np} and decreased with increasing δ_{np} for projectiles with thicker neutron skins. For fragments within the range $A_f \leq 90\% A_P$, the trend of the $S_A[f]$ distribution was similar to that of $A_f \leq 14$, indicating that $S_A[f]$ was significantly influenced by the selected range of fragments. Compared with the $S_A[f] \sim \delta_{np}$ correlation reported in [11], the results for $15 \leq A_f \leq 90\% A_P$ are in good agreement, in which $S_A[f]$ decreased linearly with increasing δ_{np} of the neutron-rich projectile nucleus. It is suggested that the adopted range of fragments significantly influences $S_A[f]$ as well as the $S_A[f] \sim \delta_{np}$ correlation. If the fragments are limited to relatively small sizes, the obtained CIE may be insensitive to the neutron skin thickness if it is not very thick. Large fragments, which are produced in peripheral collisions and are influenced by neutron skin structures, better reflect information about neutron skin thickness.

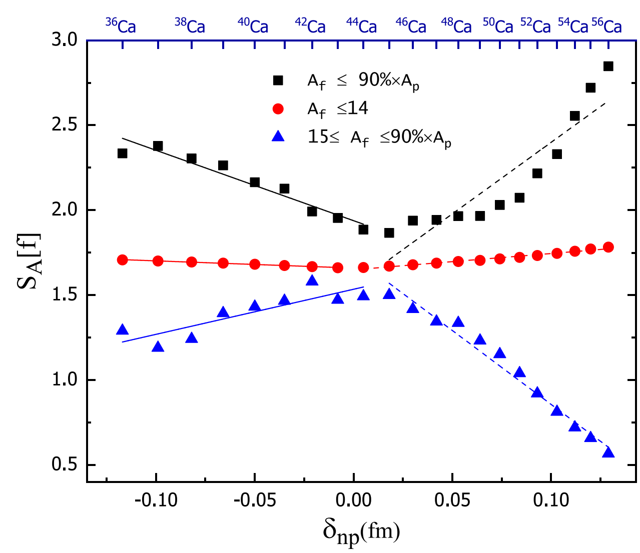

Fig. 5 (Color online) CIE ($S_A[f]$) correlation to neutron skin thickness (δ_{np}) of projectile nuclei $^{36-56}$Ca. The quantities of $S_A[f]$ are determined from different ranges of fragments, for which the squares, circles, and triangles denote $S_A[f]$ determined from the fragment mass within $A_f \leq 90\% A_P$, $A_f \leq 14$, and $15 \leq A_f \leq 90\% A_P$, respectively. Linear fittings (lines) are performed on the $S_A[f] \sim \delta_{np}$ correlations according to $\delta_{np} < 0$ and $\delta_{np} > 0$

4 Conclusion

CIE analysis was adopted to quantify the CIE incorporated in the fragment σ_A distributions of PF reactions. The newly proposed BNN + FRACS model was used to predict the fragment σ_A distributions in the 140 MeV/u $^{36-56}$Ca + ^{9}Be reactions. The neutron skin thickness of the projectile nuclei was calculated using Fermi-type nuclear density distributions for protons and neutrons. By performing an FFT analysis of fragment σ_A distributions, $F(k)$ distributions were obtained and further used to determine the CIE included in the fragment distributions. The influence of fragment size on the CIE was investigated by setting different upper limitations on the fragment mass according to different percentages of $A_{\mathrm{f}}/A_{\mathrm{P}}$. It is concluded that the range of fragments influences the quantity of CIE and exhibits different correlations with the neutron skin thickness of the projectile nucleus, which are as follows:

- The CIE $S_A[f]$ was not sensitive to the neutron skin thickness if the upper limitations on the fragments were relatively small, for example, $A_{\mathrm{f}} \leq 75\% A_{\mathrm{P}}$ and less, for which the roots in the neutron skin were mainly influenced by the diffuseness of the nucleus.
- When relatively large mass fragments were included to determine $S_A[f]$, for neutron-deficient projectile nuclei, $S_A[f]$ exhibited a decreasing trend with increasing δ_{np}, whereas it increased with δ_{np} for neutron-rich projectile nuclei.
- By dividing the fragments into two groups according to their mass numbers, that is, the relatively light fragments of $A_{\mathrm{f}} \leq 14$ and the relatively large fragments of $15 \leq A_{\mathrm{f}} \leq 90\% A_{\mathrm{P}}$, $S_A[f]$ was found to have different types of correlations with δ_{np} of the projectile nucleus.
- The CIE determined from fragments of $15 \leq A_{\mathrm{f}} \leq 90\% A_{\mathrm{P}}$ reproduced the trend of a previous correlation obtained in [11], showing a good linear $S_A[f] \sim \delta_{\mathrm{np}}$ correlation in the neutron-rich projectile nuclei of calcium isotopes.

These results indicate that although the $S_A[f] \sim \delta_{\mathrm{np}}$ relationship may be significantly influenced by light mass fragments, the correlation between them is very weak. Thus, the use of large-mass fragments is proposed to study the $S_A[f] \sim \delta_{\mathrm{np}}$ correlation for neutron-rich projectile nuclei.

Acknowledgements We thank Prof. Chun-Wang Ma for his suggestion to study this topic.

Author Contributions All authors contributed to the study conception and design. Material preparation, data collection, and analysis were performed by Xun Zhu, Chen Yuan, and Hui-Ling Wei. The first draft of the manuscript was written by Hui-Ling Wei and all authors commented on previous versions of the manuscript. All authors read and approved the final manuscript.

References

1. J. Meng, P. Ring, Giant Halo at the neutron drip line. Phys. Rev. Lett. **80**, 460 (1998). https://doi.org/10.1103/PhysRevLett.80.460
2. J. Meng, H. Toki, S.G. Zhou et al., Relativistic continuum Hartree Bogoliubov theory for ground-state properties of exotic nuclei. Prog. Part. Nucl. Phys. **57**, 470 (2006). https://doi.org/10.1016/j.ppnp.2005.06.001
3. J. Meng, S.G. Zhou, Halos in medium-heavy and heavy nuclei with covariant density functional theory in continuum. J. Phys. G Nucl. Part. Phys. **42**, 093101 (2015). https://doi.org/10.1088/0954-3899/42/9/093101
4. C.W. Ma, H.L. Wei, X.Q. Liu et al., Nuclear fragments in projectile fragmentation reactions. Prog. Part. Nucl. Phys. **121**, 103911 (2021). https://doi.org/10.1016/j.ppnp.2021.103911
5. C.W. Ma, Y.G. Ma, Shannon information entropy in heavy-ion collisions. Prog. Part. Nucl. Phys. **99**, 120 (2018). https://doi.org/10.1016/j.ppnp.2018.01.002
6. C.W. Ma, Y. Fu, D.Q. Fang et al., A possible experimental observable for the determination of neutron skin thickness. Chin. Phys. B **17**, 1216 (2008). https://doi.org/10.1088/1674-1056/17/4/011
7. C.W. Ma, H.L. Wei, Y.G. Ma, Neutron-skin effects in isobaric yield ratios for mirror nuclei in a statistical abrasion-ablation model. Phys. Rev. C **88**, 044612 (2013). https://doi.org/10.1103/PhysRevC.88.044612
8. T. Aumann, C.A. Bertulani, F. Schindler et al., Peeling off neutron skins from neutron-rich nuclei: Constraints on the symmetry energy from neutron-removal cross sections. Phys. Rev. Lett. **119**, 262501 (2017). https://doi.org/10.1103/PhysRevLett.119.262501
9. L. Li, F.-Y. Wang, Y.-X. Zhang, Isospin effects on intermediate mass fragments at intermediate energy-heavy ion collisions. Nucl. Sci. Tech. **33**, 58 (2022). https://doi.org/10.1007/s41365-022-01050-w
10. C.C. Guo, J. Su, L. Zhu, Secondary decay effects of the isospin fractionation in the projectile fragmentation at GeV/nucleon. Nucl. Sci. Tech. **31**, 123 (2020). https://doi.org/10.1007/s41365-020-00832-4
11. C.W. Ma, Y.P. Liu, H.L. Wei et al., Determination of neutron-skin thickness using configurational information entropy. Nucl. Sci. Tech. **33**, 6 (2022). https://doi.org/10.1007/s41365-022-00997-0
12. B. Mei, Improved empirical parameterization for projectile fragmentation cross sections. Phys. Rev. C **95**, 034608 (2017). https://doi.org/10.1103/PhysRevC.95.034608
13. C.W. Ma, X.B. Wei, X.X. Chen et al., Precise machine learning models for fragment production in projectile fragmentation reactions by Bayesian neural networks. Chin. Phys. C **46**, 074104 (2022). https://doi.org/10.1088/1674-1137/ac5efb
14. C.W. Ma, D. Peng, H.L. Wei et al., Isotopic cross-sections in proton induced spallation reactions based on the Bayesian neural network method. Chin. Phys. C **44**, 014104 (2020). https://doi.org/10.1088/1674-1137/44/1/014104
15. C.W. Ma, D. Peng, H.L. Wei et al., A Bayesian-neural-network prediction for fragment production in proton induced spallation reaction. Chin. Phys. C **44**, 124107 (2020). https://doi.org/10.1088/1674-1137/abb657
16. D. Peng, X.X. Chen, H.L. Wei et al., Bayesian evaluation of residual production cross sections in proton-induced nuclear

spallation reactions. J. Phys. G Nucl. Part. Phys. **49**, 085102 (2022). https://doi.org/10.1088/1361-6471/ac7069
17. A.E. Bernardini, R. da Rocha, Entropic information of dynamical AdS/QCD holographic models. Phys. Lett. B **762**, 107 (2016). https://doi.org/10.1016/j.physletb.2016.09.023
18. W. Rubin, *Real and Complex Analysis* (McGrawChill, Singapore, 1987)
19. C.E. Shannon, A mathematical theory of communication. Bell Syst. Tech. J. **27**, 379 (1948). https://doi.org/10.1002/j.1538-7305.1948.tb01338.x
20. K. Sümmerer, Improved empirical parametrization of fragmentation cross sections. Phys. Rev. C **86**, 014601 (2012). https://doi.org/10.1103/PhysRevC.86.014601
21. M. Mocko, M.B. Tsang, L. Andronenko et al., Projectile fragmentation of ^{40}Ca, ^{48}Ca, ^{58}Ni, and ^{64}Ni at 140 MeV/nucleon. Phys. Rev. C **74**, 054612 (2006). https://doi.org/10.1103/PhysRevC.74.054612